TWO-DIMENSIONAL DISK DYNAMOS WITH VERTICAL OUTFLOWS INTO A HALO

B. VON REKOWSKI, W. DOBLER AND A. SHUKUROV
Department of Mathematics, University of Newcastle
Merz Court, Newcastle upon Tyne NE1 7RU, UK

AND

A. BRANDENBURG
Nordita, Blegdamsvej 17, DK-2100 Copenhagen Ø, Denmark

Abstract. We study the effects of vertical outflows on mean-field dynamos in disks. These outflows could be due to thermal winds or magnetic buoyancy. We analyse numerical solutions of the nonlinear mean-field dynamo equations using a two-dimensional finite-difference model. Contrary to expectations, a modest vertical velocity can enhance dynamo action. This can lead to super-exponential growth of the magnetic field and to higher magnetic energies at saturation in the nonlinear regime.

1. Introduction

Large scale magnetic fields are often considered to be an important factor in accretion disks (including generation of turbulence), crucial in launching winds or jets. The origin of such large scale magnetic fields in accretion disks is still unclear: they may be advected from the surrounding medium or be generated by a dynamo inside the disk. Advection appears unlikely as turbulence leads to enhanced viscosity and magnetic diffusivity, so that the two are of the same order, i.e. the magnetic Prandtl number is of order unity [1]. In this case the turbulent magnetic diffusivity can compensate the dragging of the field by viscously induced accretion flow [2, 3, 4]. Turbulent dynamo action is a plausible mechanism for producing large scale magnetic fields in accretion disks [5, 6]. Dynamo magnetic fields can launch winds from accretion disks [7, 8, 9]. However, the wind can also affect the dynamo. In particular, a dynamo enhancement by winds was suggested earlier for

galactic dynamos [10]. In the same context the effects of shear in the vertical velocity on the dynamo was considered [11].

We assume here that the magnetic fields are generated by a dynamo acting in a relatively thin accretion disk. We show how vertical flow can enhance the dynamo, allowing for a larger growth rate and leading to super-exponential growth of the magnetic field and to enhanced saturation levels of magnetic energy.

The vertical velocities can have several origins. For example, they can be due to a thermally driven wind emanating from the disk or magnetic buoyancy in the disk. Note that here we invoke magnetic buoyancy as a driver of vertical outflows; it can itself contribute to the dynamo effect [12], but such effects are not taken into account here.

2. The model

The equation which we solve is the mean-field induction equation which we evolve in terms of the vector potential $\mathbf{A}$, where $\mathbf{B} = \nabla \times \mathbf{A}$,

$$\frac{\partial \mathbf{A}}{\partial t} = \mathbf{V} \times (\nabla \times \mathbf{A}) + \alpha \nabla \times \mathbf{A} - \eta \mu_0 \mathbf{j}, \tag{1}$$

where $\mathbf{j} = \nabla \times \mathbf{B}/\mu_0$ is the current density, μ_0 the magnetic permeability, η the turbulent magnetic diffusivity, α the α-effect and $\mathbf{V}$ the mean velocity. We neglect the radial component of the mean velocity. Assuming the α- and η-tensors to be isotropic, we can consider scalar quantities. We do not make the thin-disk approximation but solve the general equations. We adopt cylindrical coordinates (r, φ, z) and restrict ourselves to axisymmetric solutions. Equation (1) is solved using a sixth order finite-difference scheme in space and a third order Runge-Kutta time advance scheme.

Our computational domain contains a disk embedded in its surrounding halo. We take a disk aspect ratio of $h_{\rm disk}/R_{\rm disk} = 0.1$ and a halo with $h_{\rm halo}/h_{\rm disk} \approx 6$.

As an initial condition for the magnetic field we choose a purely poloidal field in the disk of either dipolar or quadrupolar symmetry.

On the boundaries of the computational domain we impose pseudo-vacuum conditions. However, since the boundaries are in the halo far away from the disk, the choice of boundary conditions is not crucial.

The α-coefficient $\alpha(r, z)$ is antisymmetric about the disk midplane and vanishes outside the disk. We adopt

$$\alpha(r,z) = \begin{cases} \alpha_0(r) \sin\left(\pi \frac{z}{h}\right) \xi_\alpha(r) & \text{for } |z| \le h, \\ 0 & \text{for } |z| > h. \end{cases} \tag{2}$$

The ξ_α-profile cuts off the α-effect at the outer radius of the disk as well as at an inner radius, where the rotational shear is very strong.

As appropriate for accretion disks, we adopt a softened Keplerian angular velocity profile in r in the disk as well as the halo,

$$\Omega(r) = \sqrt{\frac{GM}{r^3}} \left[1 + \left(\frac{r_0}{r}\right)^n\right]^{-\frac{n+1}{2n}}, \tag{3}$$

where G is Newton's gravitational constant, M is the mass of the central object, $r_0 = 0.05$ is the softening radius, and $n = 5$. At $r = 0$, Ω vanishes.

The turbulent magnetic diffusivity is given by

$$\eta(r, z) = \eta_{\rm halo} + (\eta_{\rm disk} - \eta_{\rm halo})\xi(r, z). \tag{4}$$

The profile $\xi(r, z)$ defines the disk: ξ is equal to unity inside the disk and vanishes in the halo but with a smooth transition between. We carried out computations for two cases: homogeneous conductivity, $\eta_{\rm halo}/\eta_{\rm disk} = 1$, and low conductivity in the halo, $\eta_{\rm halo}/\eta_{\rm disk} = 20$.

The profile for V_z is linear in z, $V_z(z) = V_{z0}z/h$, where V_{z0} is a characteristic vertical velocity.

Our dynamo problem is controlled by the three magnetic Reynolds numbers related to the α-effect, the differential rotation and the vertical velocity,

$$R_\alpha = h\alpha_0/\eta_{\rm disk}, \quad R_\omega = h^2 S/\eta_{\rm disk}, \quad R_v = hV_{z0}/\eta_{\rm disk}, \tag{5}$$

where $S(r) \equiv r d\Omega/dr \approx -3/2\ \Omega(r)$ is the rotational shear. The dynamo number is defined as $\mathcal{D} \equiv R_\alpha R_\omega$. Since the dynamo number is approximately constant, $|\mathcal{D}| \simeq \alpha_{\rm SS}^{-2} \simeq 10^2 - 10^4$ in thin accretion disks [5], we assume $\mathcal{D}$ to be constant by setting $\alpha_0(r) = \mathcal{D}\eta_{\rm disk}^2/S(r)h^3$.

Because of the strong differential rotation we assume that the magnetic field in the disk is generated by a standard $\alpha\omega$-dynamo. The two control parameters are then the dynamo number $\mathcal{D}$ and the vertical magnetic Reynolds number R_v. The value of R_v obviously depends on the origin of the vertical outflow. With magnetic buoyancy, a rough estimate can be done assuming that the vertical velocities are comparable to the Alfvén speed. Estimating the Alfvén speed from magnetic equipartition, one gets a vertical magnetic Reynolds number R_v of order unity.

3. Linear results for $R_v = 0$

For $\eta_{\rm halo} = \eta_{\rm disk}$, the growth rates of dipolar and quadrupolar modes should be exchanged when $\mathcal{D}$ reverses sign, i.e. the graph of $Re(\gamma)$ as a function of $\mathcal{D}$ should be symmetric with respect to the vertical axis $\mathcal{D} = 0$ with quadrupolar and dipolar modes exchanging their rôles [13]. Our numerical simulation shows this symmetry with a good precision (Fig. 1a). This is because the ratio between $h_{\rm halo}$ and $h_{\rm disk}$ is large enough, about 6.

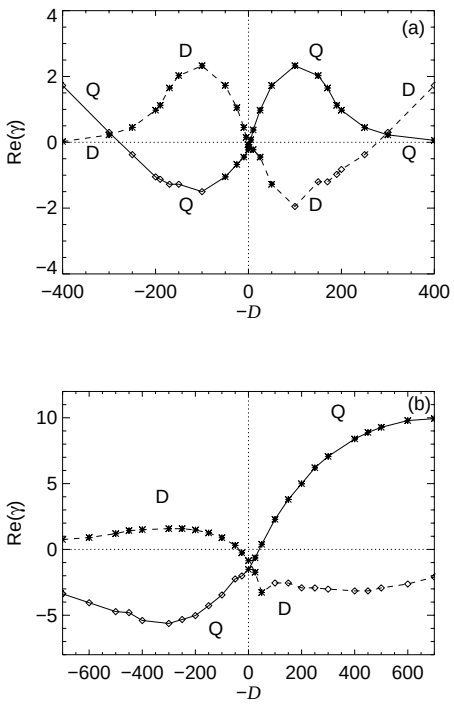

Figure 1. Real part of the growth rate of the magnetic field as a function of $-\mathcal{D}$ with $R_v = 0$. Asterisks denote non-oscillatory, diamonds oscillatory solutions. Solid lines denote quadrupolar (Q), dashed lines dipolar (D) modes. (a) is with homogeneous conductivity, (b) for low-conducting halo. Note the symmetry of (a) with respect to $\mathcal{D} = 0$.

For $\mathcal{D} < 0$ ($R_\alpha > 0$) the first leading growing mode is quadrupolar whereas for $\mathcal{D} > 0$ ($R_\alpha < 0$) it is dipolar; both are non-oscillatory. We thus study the effect of vertical velocities for $\mathcal{D} < 0$ in quadrupolar and for $\mathcal{D} > 0$ in dipolar symmetry at dynamo numbers up to ± 300.

For $\eta = \text{const.}$, the critical dynamo number is $|\mathcal{D}_{\rm crit}| \simeq 5$. The dominant mode changes its symmetry and becomes oscillatory at $|\mathcal{D}| \simeq 300$.

The qualitative behaviour in the case of low conductivity in the halo is quite similar to that of homogeneous conductivity. Also the quadrupolar non-oscillatory modes first become dominant for $R_\alpha > 0$ and the dipolar non-oscillatory modes for $R_\alpha < 0$ (compare Figs. 1a and b).

But there are quantitative differences. The value of $|\mathcal{D}|$, where the symmetry of the leading mode changes, is larger than 700. Also, the diagram in Fig. 1b is not symmetric. The critical dynamo number is $\mathcal{D} \simeq -50$ (50) for quadrupolar (dipolar) modes.

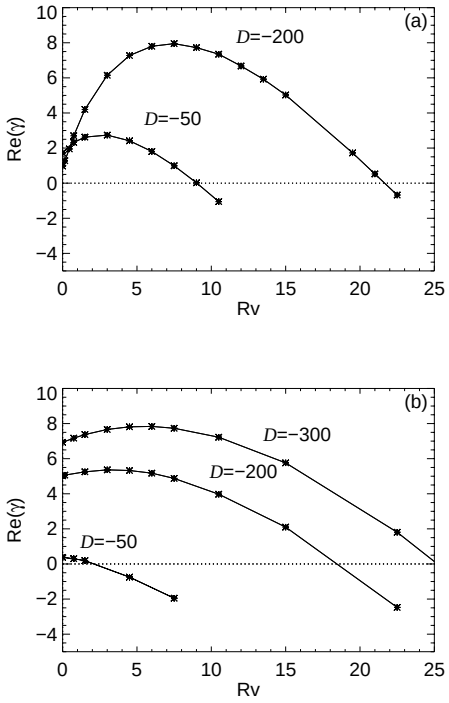

Figure 2. Real part of the growth rate of the magnetic field as a function of R_v for non-oscillatory quadrupolar modes. (a) $\eta_{\rm halo}/\eta_{\rm disk} = 1$, (b) $\eta_{\rm halo}/\eta_{\rm disk} = 20$.

4. Linear behaviour with vertical velocities

As discussed in section 3, we only consider quadrupolar symmetry for $\mathcal{D} < 0$. As shown in Fig. 2, the growth rate of the magnetic field $\mathrm{Re}(\gamma)$ is a non-monotonous function of R_v, for $\eta_{\rm halo}/\eta_{\rm disk}$ equal to both 1 and 20. A maximum in $\mathrm{Re}(\gamma)$ occurs, however, only for $|\mathcal{D}|$ large enough, and the smaller the magnetic diffusivity of the halo, the smaller is the required $|\mathcal{D}|$. The larger $|\mathcal{D}|$, the more pronounced is the maximum. The maximum growth rate occurs for R_v of the order of 1 to 10.

In Fig. 3 we show the effect of the dynamo number and the vertical velocity on the magnetic field configuration for $\eta_{\rm halo} = \eta_{\rm disk}$. Increasing $|\mathcal{D}|$ from 50 to 200 in the absence of any vertical velocity results in the magnetic field becoming concentrated at larger radii in the disk (Fig. 3a and b).

As can be seen in Fig. 3b, c and d, a vertical velocity with $R_v < 7.5$ leads to a wider vertical distribution of magnetic field which reduces magnetic diffusion and enhances the dynamo action. At still larger R_v, the wind

aligns the poloidal field lines with the lines of constant rotation, and the Ω-effect is slowly switched off leading to a decrease in the growth rate, which eventually becomes negative. The mode structures at a maximum of $\mathrm{Re}(\gamma)$, reached at $R_v = 7.5$ for $\mathcal{D} = -200$) and $R_v = 3$ for $\mathcal{D} = -50$, are very similar to each other.

The growth rate for dipolar non-oscillatory modes ($\mathcal{D} > 0$) has no maximum as R_v increases; at R_v of order 1 or even less the dynamo is switched off. The magnetic field is advected outwards and aligned with the Ω-contour lines in vertical direction very quickly.

5. Nonlinear behaviour with vertical velocities

We consider nonlinear, saturated solutions in a model with homogeneous conductivity, $\eta_{\rm halo} = \eta_{\rm disk}$, negative dynamo number and quadrupolar symmetry (the dominant symmetry for moderate $|\mathcal{D}|$ with $R_v = 0$). All saturated magnetic fields are non-oscillatory, as the corresponding linear modes.

5.1. MAGNETIC BUOYANCY

We parameterize the effect of magnetic buoyancy by assuming the vertical velocity to be proportional to the maximum magnetic field strength. Thus, the vertical magnetic Reynolds number becomes time-dependent,

$$R_v = R_{v0} \max_{\mathbf{x}}(B_r, B_\varphi)/|B_0|, \quad R_{v0} \equiv V_{z0} h/\eta_{\rm disk}, \tag{6}$$

where B_0 is a characteristic field strength.

As time increases, $|\mathbf{B}|$ grows and therefore R_v is increasing and the growth rate follows, e.g., the upper curve in Fig. 2a for $\mathcal{D} = -200$. Thus, as long as R_v is less than the position of the γ-maximum, γ increases with time, which results in a super-exponential growth. After the maximum, at $R_v = 7.5$, γ decreases and eventually the magnetic field approaches its saturation level. This is reached when $R_v = R_{v*}$, where R_{v*} is the zero of $\gamma(R_v)$. According to Eq. (6), the saturation value of magnetic energy will thus be $E_{\rm mag} \propto 1/R_{v0}^2$.

5.2. α-QUENCHING

We consider the back-reaction of the magnetic field on the α-effect, introducing the nonlinearity $1/(1 + B^2/B_{\rm eq}^2)$ as a factor in the α-effect; $B_{\rm eq}$ is the equipartition field.

The magnetic energy has a maximum at a certain value of R_v (Fig. 4, left), but this maximum occurs at $R_v \approx 0.1$, a value smaller than where a maximum of $\mathrm{Re}(\gamma)$ occurs in the linear regime, and it is also less pro-

nounced. The value of R_v where the maximum occurs, is independent of $\mathcal{D}$. The magnetic energy scales roughly with the dynamo number, $E_{\rm mag} \propto \mathcal{D}$.

The effect of vertical velocity on the magnetic field for the model with α-quenching is shown in Fig. 5; the structure changes only weakly with the dynamo number. With increasing R_v the poloidal field lines become vertical, i.e. aligned with the lines of constant rotation. Hence, shear has no effect, and the Ω-effect is switched off, as in the linear model.

5.3. α-QUENCHING TOGETHER WITH MAGNETIC BUOYANCY

When α-quenching and magnetic buoyancy are combined, the vertical magnetic Reynolds number depends on position and time and takes the form $R_v = R_{v0}\sqrt{B_r^2 + B_\varphi^2}/|B_{\rm eq}|$. Without α-quenching, since R_v is now nonlocal, the temporal behaviour of the growth rates at short times does not have to be super-exponential. Surprisingly, again we find $E_{\rm mag} \propto 1/R_{v0}^2$ (see Fig. 4, right, dashed line).

In the second panel of Fig. 4 magnetic energy is plotted against R_v for $\mathcal{D} = -50$ for the three nonlinear models. α-quenching appears to be the dominant nonlinearity in the model considered.

Acknowledgements

We acknowledge financial support from PPARC (Grant PPA/G/S/1997/00284) and the Leverhulme Trust (Grant F/125/AL). The use of the PPARC supported GRAND parallel computer is acknowledged.

References

1. Pouquet, A., Frisch, U. and Léorat, J. (1976) Strong MHD helical turbulence and the nonlinear dynamo effect, *J. Fluid. Mech.*, **77**, 321–354
2. van Ballegooijen, A.A. (1989) Magnetic fields in the accretion disks of cataclysmic variables, *in G. Belvedere (ed.), Accretion disks and magnetic fields in astrophysics, Kluwer Academic Publishers*, 99–106
3. Lubow, S.H., Papaloizou, J.C.B. and Pringle, J.E. (1994) Magnetic field dragging in accretion discs, *MNRAS*, **267**, 235–240
4. Heyvaerts, J., Priest, E.R. and Bardou, A. (1996) Magnetic field diffusion in self-consistently turbulent accretion disks, *ApJ*, **473**, 403–421
5. Pudritz, R.E. (1981) Dynamo action in turbulent accretion discs around black holes – II. The mean magnetic field, *MNRAS*, **195**, 897–914
6. Stepinski, T.F. and Levy, E.H. (1988) Generation of dynamo magnetic fields in protoplanetary and other astrophysical accretion disks, *ApJ*, **331**, 416–434
7. Campbell, C.G., Papaloizou, J.C.B. and Agapitou, V. (1998) Magnetic field bending in accretion discs with dynamos, *MNRAS*, **300**, 315–320
8. Campbell, C.G. (1999) Launching of accretion disc winds along dynamo-generated magnetic fields, *MNRAS*, **310**, 1175–1184
9. Brandenburg, A., Dobler, W., Shukurov, A. and von Rekowski, B. (2000) Pressure-driven outflow from a dynamo active disc, *A&A*, submitted

10. Brandenburg, A., Donner, K.J., Moss, D., Shukurov, A., Sokoloff, D.D. and Tuominen, I. (1993) Vertical magnetic fields above the discs of spiral galaxies, *A&A*, **271**, 36–50
11. Elstner, D., Golla, G., Rüdiger, G. and Wielebinski, R. (1995) Galactic halo magnetic fields due to a 'spiky' wind, *A&A*, **297**, 77–82
12. Moss, D., Shukurov, A. and Sokoloff, D. (1999) Galactic dynamos driven by magnetic buoyancy, *A&A*, **343**, 120–131
13. Proctor, M.R.E. (1977) On the eigenvalues of kinematic alpha-effect dynamos, *Astron. Nachr.*, **298**, 19–25

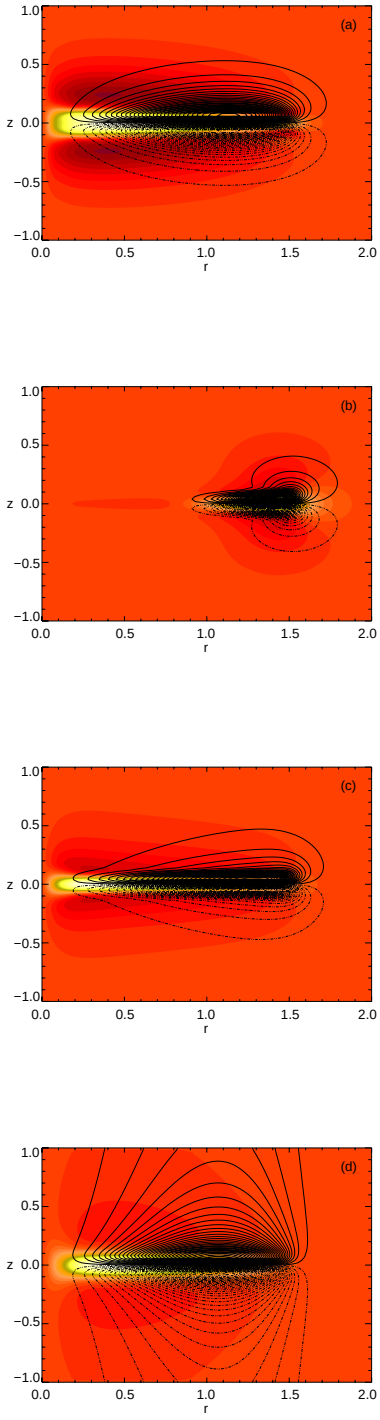

Figure 3. The effect of dynamo number and vertical velocity on the magnetic field configuration, for the linear model with $\eta_{\rm halo} = \eta_{\rm disk}$. Shown are the poloidal field lines (solid is clockwise, dotted is counter-clockwise) and the toroidal field (grey scales: bright is in positive, dark in negative azimuthal direction). (a): $\mathcal{D} = -50$, $R_v = 0$; (b): $\mathcal{D} = -200$, $R_v = 0$; (c): $\mathcal{D} = -200$, $R_v = 0.75$; (d): $\mathcal{D} = -200$, $R_v = 7.5$ (where Re(γ) is maximum). Comparing (a) and (b) shows the effect of increasing $\mathcal{D}$ while $R_v = 0$. Panels (b) to (d) follow the upper curve in Fig. 2a. All modes are quadrupolar and non-oscillatory.

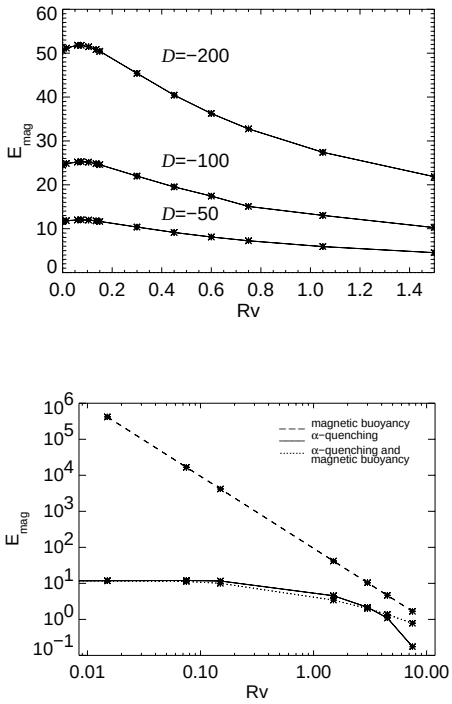

Figure 4. Magnetic energy as a function of R_v for the model with α-quenching (left) and for the models with α-quenching and/or magnetic buoyancy (right) for $\eta_{\rm halo} = \eta_{\rm disk}$. All modes are quadrupolar and non-oscillatory. The right panel shows the case $\mathcal{D} = -50$.

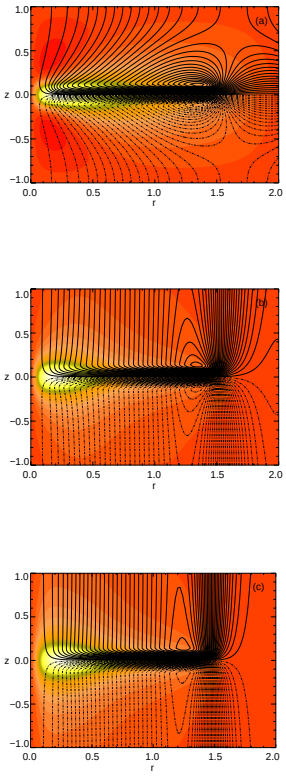

Figure 5. The effect of vertical velocity on the magnetic field configuration for the model with α-quenching and $\eta_{\rm halo} = \eta_{\rm disk}$. Shown are the poloidal field lines and the toroidal field. (a): $\mathcal{D} = -50$, $R_v = 0$; (b): $\mathcal{D} = -50$, $R_v = 3$; (c): $\mathcal{D} = -50$, $R_v = 7.5$. Panels (a) to (c) follow the lower curve in Fig. 4, left. All modes are quadrupolar and non-oscillatory.

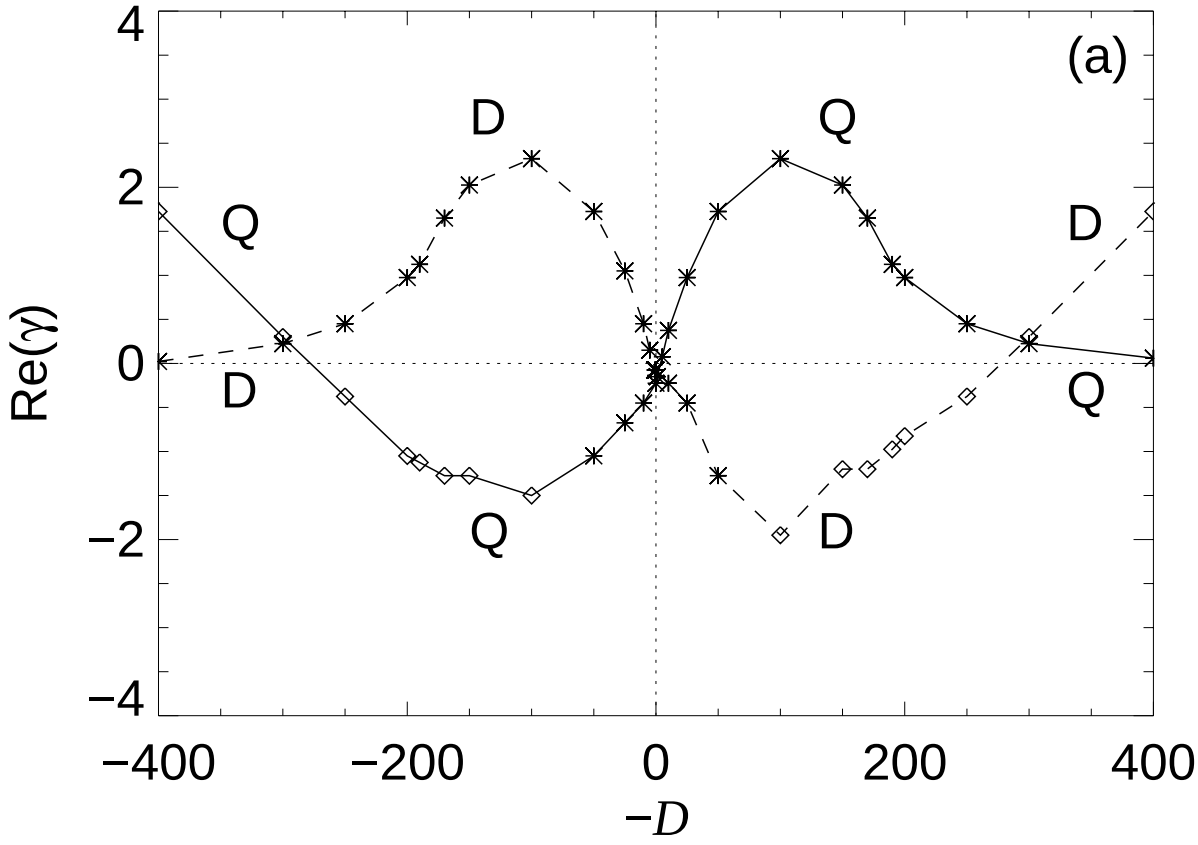
(a)
D
Q
Q
D
D
Q
Q
D
4
2
0
−2
−4
−400
−200
0
200
400
Re(γ)
−D

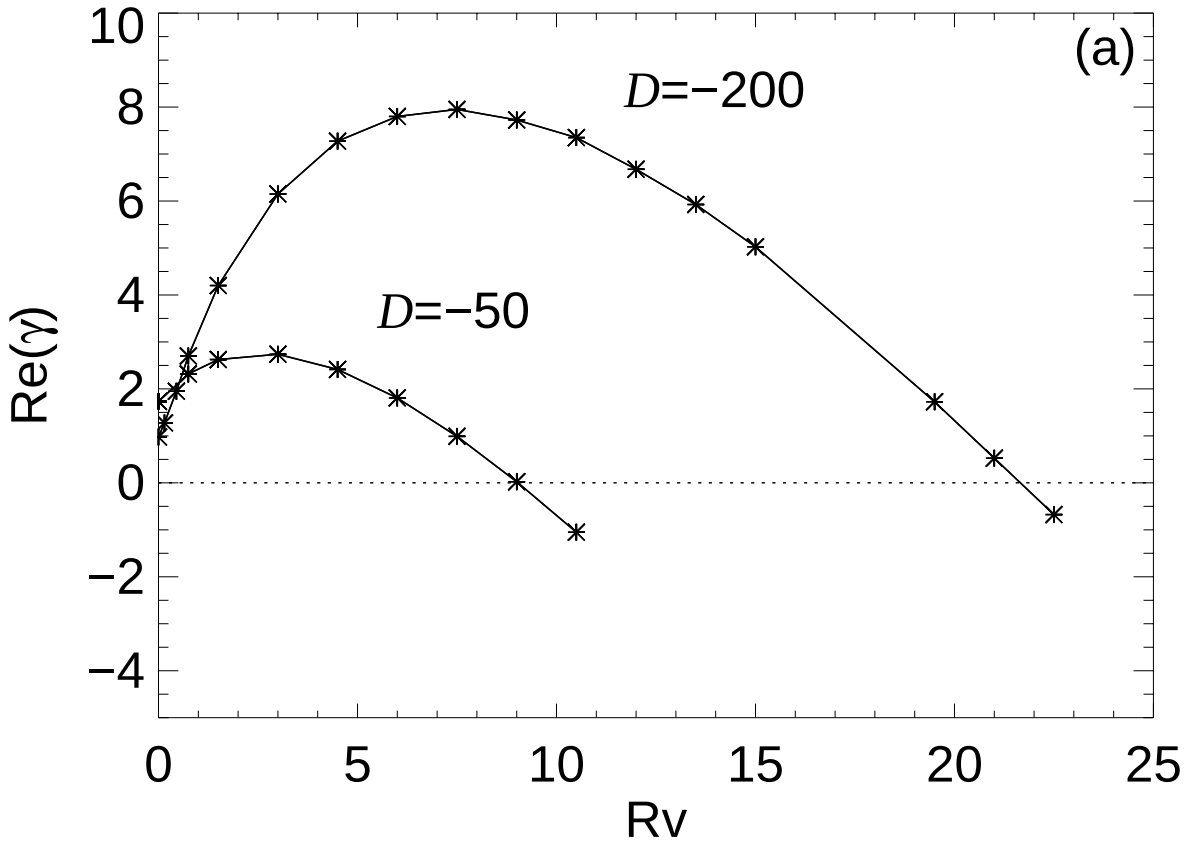
(a)
D=−200
D=−50
Re(γ)
Rv
10
8
6
4
2
0
−2
−4
0
5
10
15
20
25

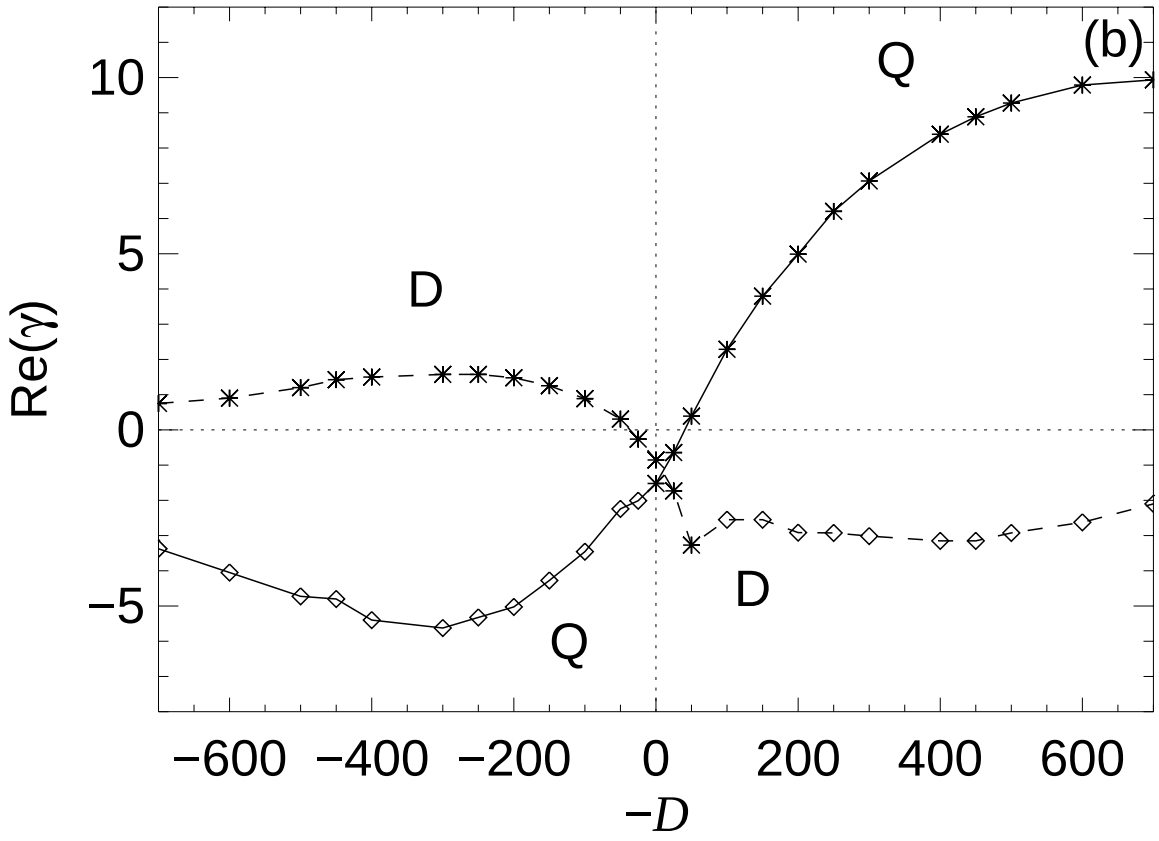
(b)
Q
D
D
Q
10
5
0
−5
Re(γ)
−600
−400
−200
0
200
400
600
−D

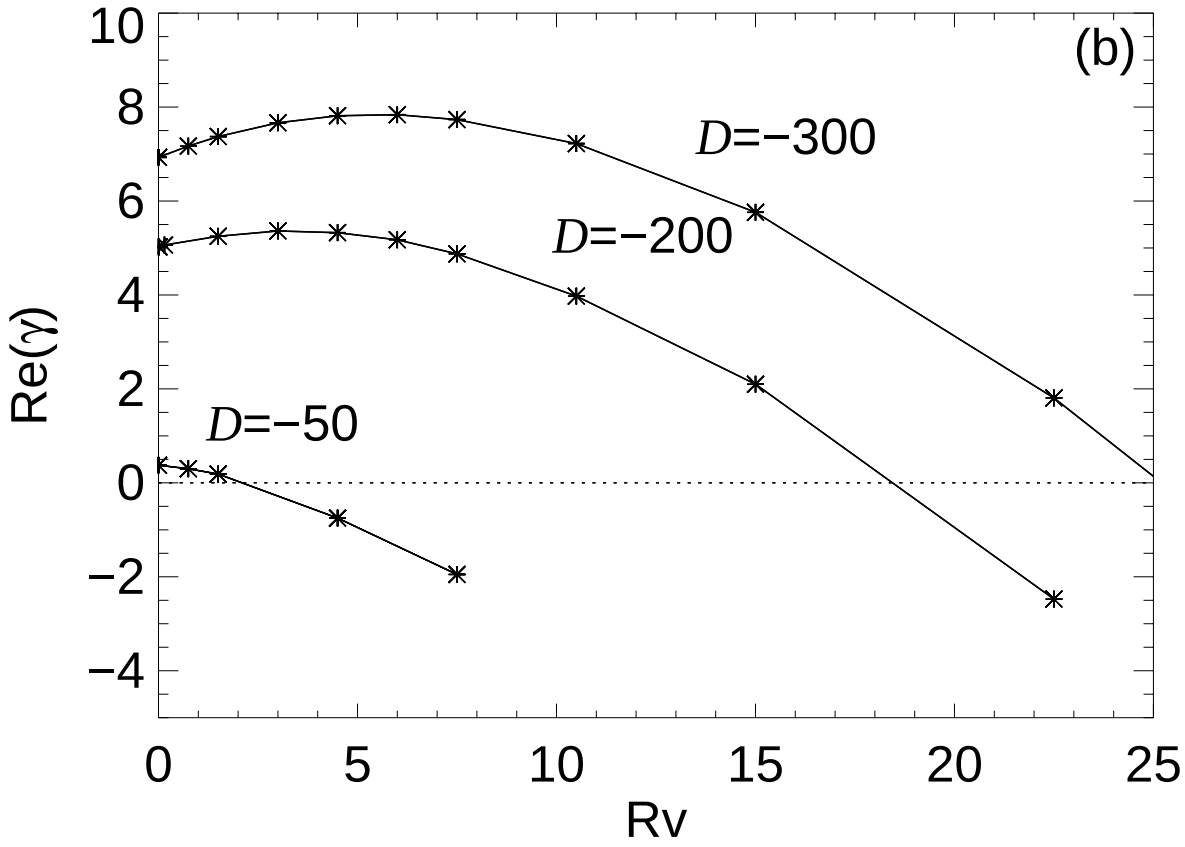
(b)
D=−300
D=−200
D=−50
Re(γ)
Rv
10
8
6
4
2
0
−2
−4
0
5
10
15
20
25

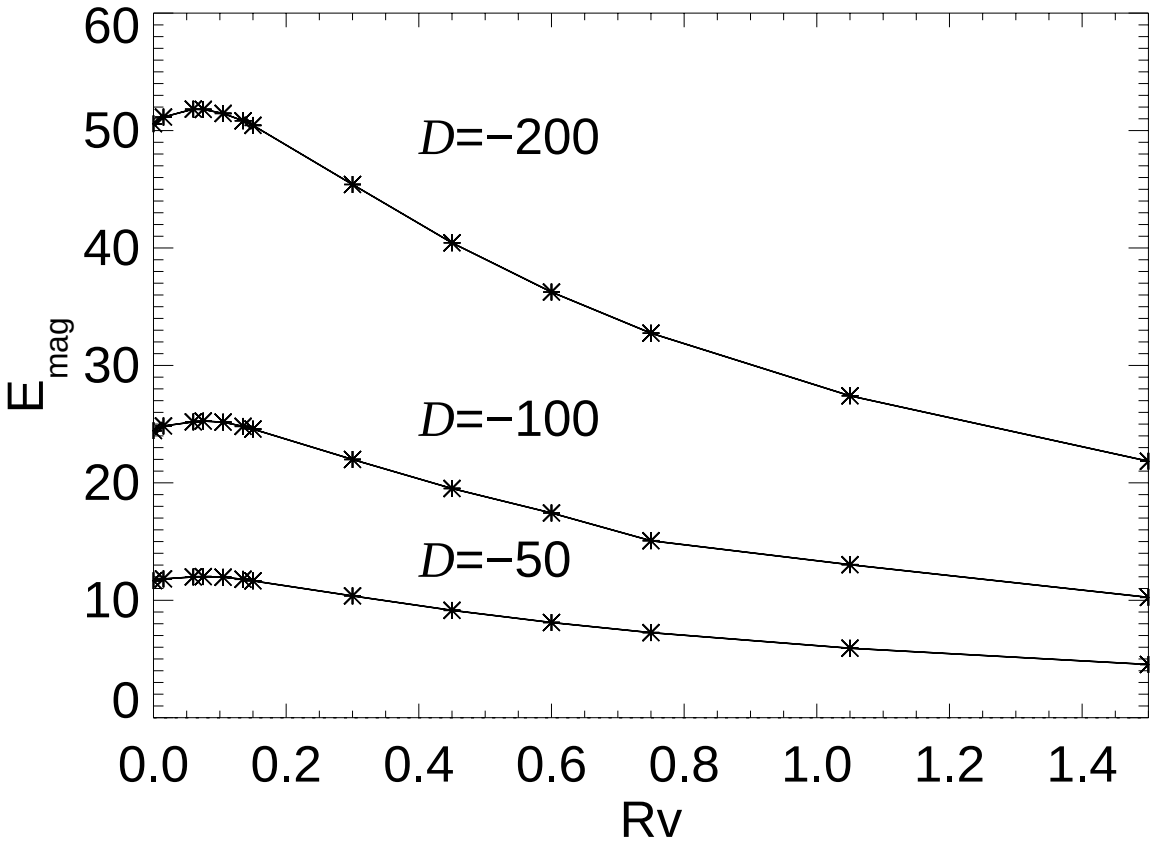
60
50
40
30
20
10
0
E mag
D=−200
D=−100
D=−50
0.0
0.2
0.4
0.6
0.8
1.0
1.2
1.4
Rv

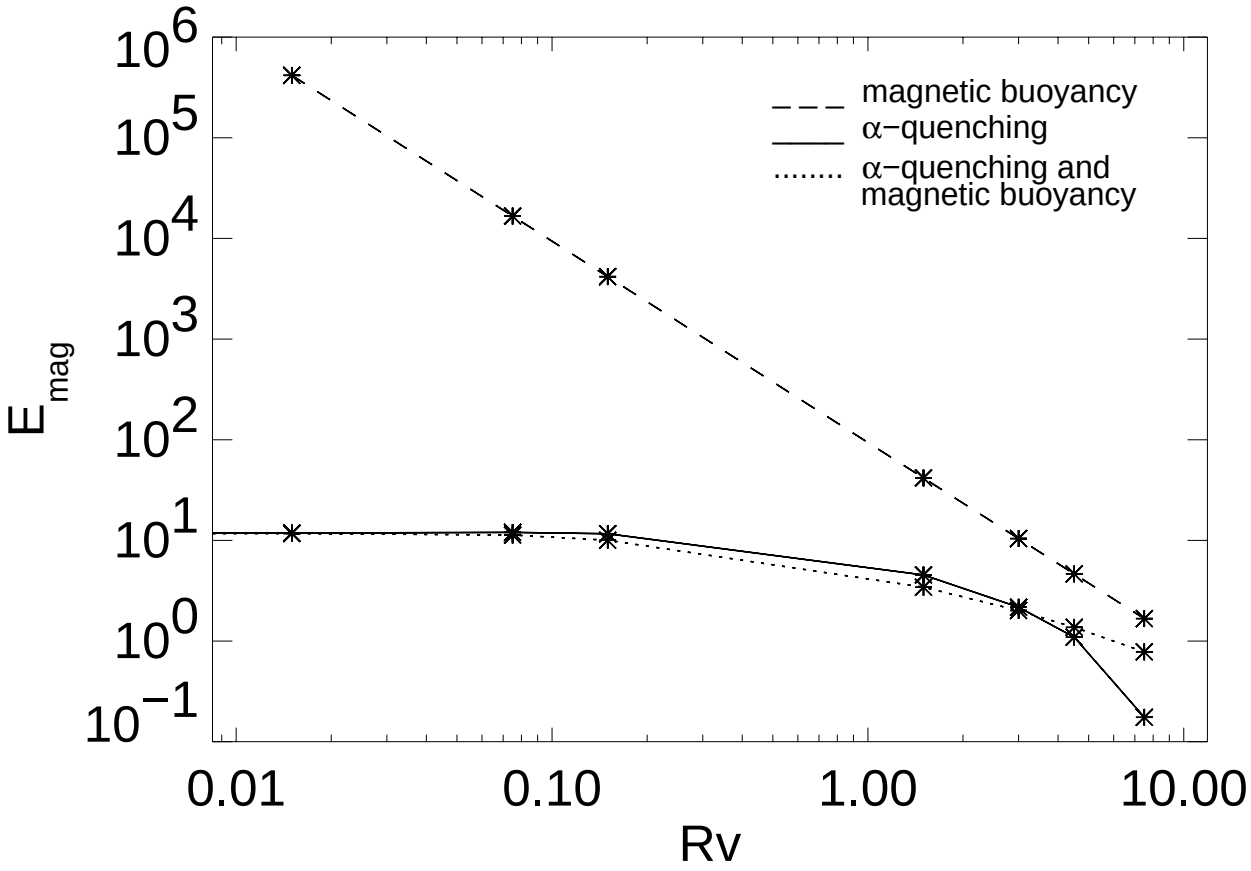
magnetic buoyancy
α−quenching
α−quenching and
magnetic buoyancy
10^6
10^5
10^4
10^3
10^2
10^1
10^0
10^{-1}
E_{mag}
0.01
0.10
1.00
10.00
Rv